Graphical analysis of current-voltage characteristics in memristive interfaces

C. Acha

Citation: Journal of Applied Physics **121**, 134502 (2017); doi: 10.1063/1.4979723
View online: http://dx.doi.org/10.1063/1.4979723
View Table of Contents: http://aip.scitation.org/toc/jap/121/13
Published by the American Institute of Physics

Graphical analysis of current-voltage characteristics in memristive interfaces

C. Acha[1,2,a)]
[1]*Universidad de Buenos Aires, Facultad de Ciencias Exactas y Naturales, Departamento de Física, Laboratorio de Bajas Temperaturas, Pabellón I, Ciudad Universitaria, C1428EHA Buenos Aires, Argentina*
[2]*CONICET – Universidad de Buenos Aires, IFIBA, Pabellón I, Ciudad Universitaria, C1428EHA Buenos Aires, Argentina*

(Received 7 November 2016; accepted 23 March 2017; published online 5 April 2017)

A graphical representation of current-voltage (IV) measurements of typical memristive interfaces at constant temperature is presented. This is the starting point to extract relevant microscopic information of the parameters that control the electrical properties of a device based on a particular metal-oxide interface. The convenience of the method is illustrated presenting some examples where the IV characteristics were simulated in order to gain insight into the influence of the fitting parameters. *Published by AIP Publishing*. [http://dx.doi.org/10.1063/1.4979723]

I. INTRODUCTION

The study of the current-voltage (IV) characteristics can be a very useful tool to understand which are the microscopic factors that determine the main conduction mechanism through metal-oxide interfaces of a device.[1,2] This microscopic knowledge may be a route to improve their capacities and a clever way to modify some specific properties. In the particular case of memristors [devices based on the resistive switching (RS) properties],[3–5] which give rise to non-volatile memories called Resistive Random Access Memories (RRAM), to understand if the resistance state (high or low) depends on electrode's or bulk's microscopic properties is an essential task in order to design their functionalities. In the case of the electrode-limited devices, the work function of the metal, the carrier affinity, and the thickness of the oxide determine the barrier height and the probability to produce an electric-field-induced-current through the junction. The conduction mechanism can then be described as Schottky (Sch), Fowler-Nordheim (FN), or direct tunneling emission. In the case of bulk-limited interfaces, the conduction mechanism is determined by the electrical properties of the oxide near the interface as, for example, those imposed by the existence of traps and their energy levels. Two examples of transport mechanisms influenced by the energy distribution and density of traps are the Poole-Frenkel (PF) emission and the space-charge-limited conduction (SCLC).

Although the IV curves are the most common way to characterize the manifestation of the RS phenomena of a device, the detailed study of its I(V) dependence on each stable state (outside the transition zone between high, low, or intermediate resistance states) would facilitate the route to determine the microscopic origin of its resistance change. In this way, their properties can be improved by optimizing the particular choice of the materials for the metal/oxide interface. As shown previously,[1,2] by analyzing the IV characteristics measured at constant temperature, it is possible to distinguish if the conduction of the device is related to an ohmic behavior ($I \sim V$), or SCLC ($I \sim V^2$), or a PF, FN, or Sch emissions [$I \sim \exp(V^n)$].

As an example of devices based on the Sch emission, we can mention those made with metal-$SrTiO_3$-metal structures[6,7] while the SCLC mechanism was encountered in Ag/$La_{0.7}Ca_{0.3}MnO_{3-\delta}$ junctions. Au/$YBa_2Cu_3O_{7-\delta}$ interfaces showed a PF conduction in a variable-range hopping scenario, with a pulse-controlled-trap energy level that determines their resistance switching properties.[8] Table I summarizes some of the basic conduction processes through metal-oxide interfaces and their I(V) dependence.

A simple way to enlighten the origin of the main conduction mechanism of a device is to plot as a function of $V^{1/2}$ the power exponent parameter γ, defined as $\gamma = dLn(I)/dLn(V)$, instead of trying to fit by trial and error their IV characteristics.[10] This is because the typical conduction mechanisms through metal-oxide interfaces have a simple γ vs $V^{1/2}$ curve (see Fig. 1): a pure ohmic, a Langmuir-Child (L-Ch), or a SCLC conduction will show a constant γ (= 1, 1.5, or 2, respectively), and a Schottky (Sch) or a Poole-Frenkel (PF) behavior is be represented by a straight line, only differing in the intercept (0 for Sch, 1 for PF). In the case of a FN conduction, a straight line with a positive slope should be obtained if γ is plotted as a function of V^{-1}.[10]

TABLE I. Examples of some basic conduction processes through metal-oxide interfaces and their I(V) dependence: FN (Fowler-Nordheim), Sch (Schottky), PF (Poole-Frenkel), and SCLC (space charge limited conduction). q is the electron's charge, ϕ_B is the barrier height, and ϕ_T is the trap energy level, $a = \sqrt{q/4\pi\epsilon' d}$, where ϵ' is the real part of the dielectric constant of the oxide and d the oxide thickness. b, A_{FN}, A_{Sch}, and A_{PF} are appropriate constants. (For more details, see Refs. 1, 2, and 9.)

Conduction process	I(V) dependence
FN	$I = A_{FN}V^2 \exp\left(\frac{-b}{V}\right)$
Sch	$I = A_{Sch}T^2 \exp\left[\frac{q}{k_bT}\left(a\sqrt{V} - \phi_B\right)\right]$
PF	$I = A_{PF}V \exp\left[\frac{q}{k_bT}\left(2a\sqrt{V} - \phi_T\right)\right]$
SCLC	$I = A_{SCLC}V^2$

a)Author to whom correspondence should be addressed. Electronic mail: acha@df.uba.ar

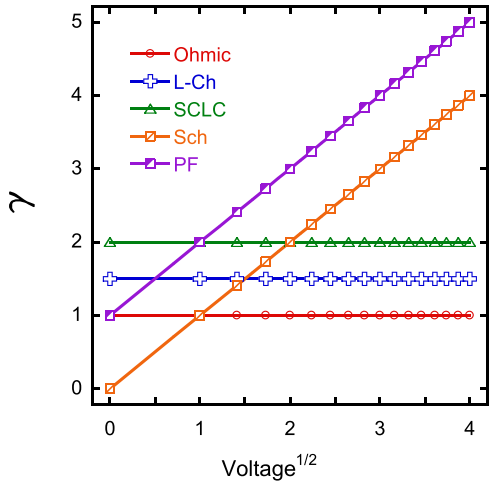

FIG. 1. The power exponent $\gamma = dLn(I)/dLn(V)$ vs $V^{1/2}$ representation of some typical conduction processes through metal-oxide interfaces: ohmic, Langmuir-Child (L-Ch), space charge limited currents (SCLC), Schottky (Sch), and Poole-Frenkel (PF).

The use of this power exponent representation has proved to be convenient for extracting physical parameters in the case of non-ideal diodes.[11] Here, we show that if a combination of conducting mechanisms are present in a particular metal-oxide interface, this representation would be very useful to graphically determine what they are. Otherwise, the standard way to do it will require the analysis of the qualities of the fits to the IV characteristics of multiple expressions to test. It should be noted that a good fit of the IV characteristics, which includes all the participating mechanisms, is essential in order to extract a flawless microscopic description of the physics behind these devices.

By considering previous works,[12–15] the combination of conduction mechanisms seems to be a common feature of bipolar memristive interfaces, as a non-linear element (NL) in parallel and/or in series with an ohmic resistor gives a convenient representation. The physical explanation of the microscopic origin of the parallel and the series structure is not clear yet. We may speculate that it can be a consequence of their capacitor-like structure where both a phase-separated interfacial zone and the proper oxide have a relevant participation in the conducting process. The interfacial zone is composed of a mixture of conducting and insulating regions,[8,14,16] probably associated with a disordered distribution of oxygen vacancies (phase separation), leading to the existence of a non-linear element in parallel with an ohmic one. The series ohmic element will then represent the bulk contribution of the oxide.

II. THE POWER EXPONENT γ REPRESENTATION

The convenience of the γ representation can be illustrated in the following examples:

As a first example, Fig. 2 shows the typical IV characteristic of an Ag-$La_{0.7}Sr_{0.3}CoO_3$ interface. Experimental details of the samples, the experimental setup, and the specific analysis of the obtained fitting parameters can be found elsewhere.[14]

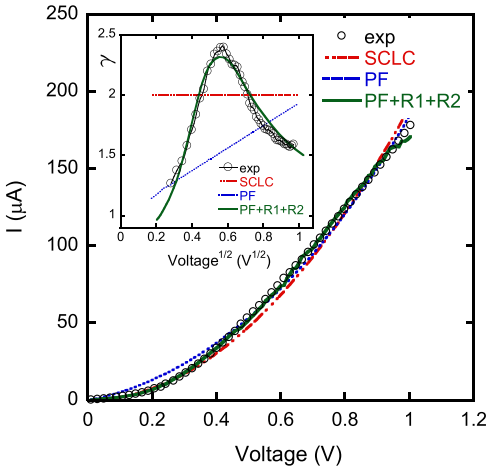

FIG. 2. IV characteristics of a Ag-cobaltite interface. Lines are fits considering a PF or a SCLC non-linear conduction and a combination of a PF conduction both in parallel with an ohmic element and in series with a second ohmic element. This latter combination of conduction processes was determined by the non-trivial γ representation of the experimental data (shown in the inset). The fitting parameters were $R_{PF}/R_1 = 700$, $R_2 = 3500\ \Omega$, and $C/T = 15\ V^{-1/2}$ (see Eqs. (4) and (5)). For comparison, the γ values of the fitting models are also represented in the inset.

A Sch mechanism can be ruled out as non-rectifying behavior was observed: although not shown here, there was no appreciable difference in the behavior of the data when comparing between the negative and the positive quadrant. The IV characteristics were fitted using the expressions of pure PF and SCLC conduction mechanisms[1,2] (see the solid lines in Fig. 2). Fits are not good and a combination of conduction mechanisms should be considered to give a right representation of the data. At this point, the way to determine which are the relevant conducting processes is somehow tedious as it requires to fit the IV data considering, by trial and error, each possible combination of the electrical conduction processes (PF or SCLC and an ohmic resistor in parallel, or with an ohmic resistor in series, or with both of them). Hopefully, the γ representation of the experimental data gives a quick graphical solution to determine the specific mechanism involved, as can be observed in the inset of Fig. 2. The γ representation of the pure PF and SCLC conduction mechanisms is clearly far from the experimental data. As we will show later (see Figs. 8 and 9), the existence of a cusp with values of $\gamma > 2$ with the tendency to reach an asymptotic value of 1 both in the low and high voltage regions is clear evidence of a PF conduction both in parallel with an ohmic element and in series with a second ohmic element (see the suggested circuit shown in Fig. 4). Then, as also shown in Fig. 2, the IV experimental data were nicely fitted with the corresponding mathematical expression for those processes. It can be seen that the γ representation of the fitting data also follows the experimental γ curve.

As a second example, Fig. 3 shows the IV characteristics of a Pt-TiO_2 (rutile)-Ti thin film device in a low resistance state and a high resistance state (LRS and HRS, respectively). The details of the synthesis, characterizations, measuring protocols, and analysis of the fitting parameters can be found elsewhere.[17] The nearly straight behavior of the IV characteristics for the LRS in the log-log plot seems to

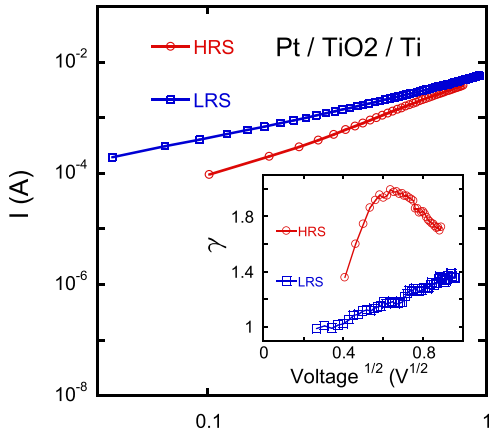

FIG. 3. IV characteristics of a Pt/TiO_2/Ti thin film device in a low resistance state and a high resistance state (LRS and HRS). The γ representation is shown in the inset, indicating that the conduction mechanism of the HRS requires a combination of a NL element (probably SCLC) both in parallel with a resistor and in series with a second resistor (see the similarity to Fig. 7). The γ representation also indicates that the LRS is not completely ohmic. Lines are guides to the eye.

indicate a power law dependence ($I \sim V^n$, with n $\simeq$ 1), while the HRS requires a more complex I(V) functional dependence. Here, as in the case of the previous example, the γ representation can be useful to understand the observed IV characteristics. As it will be analyzed in Sec. II B and II C, the shape of γ vs $V^{1/2}$ indicates a possible circuital representation of the device similar to the one described in the previous example, with a pure NL element both in parallel with a resistor and in series with a second resistor. The NL element can be associated with a SCLC behavior as $\gamma \leq 2$, but additional measurements at different temperatures should be performed to rule out a PF behavior in order to be conclusive. The LRS shows a nearly ohmic behavior, indicating that the non-linearities are still present. The RS can be interpreted by mainly considering the formation of a more conducting channel (in accordance with the experimental observations[18]), which produces a short circuit of the first resistor while producing lower changes in the other elements.

In Sec. II we will present a circuit model for bipolar memristors, whose analysis of its IV characteristics through the γ representation is greatly simplified.

A. Circuit representation for bipolar memristors

In order to gain insight into the γ representation, we propose to analyze the IV characteristics of the circuit elements shown in Fig. 4. The interfacial resistance is simulated by a pure non-linear element (NL) in parallel with an ohmic resistor R_1. The NL element can be based on the large variety of conduction mechanisms through a metal-oxide interface described in Sec. I. Here, we will analyze two particular cases of the NL element (SCLC and PF), which are common for bipolar memristors although the same analysis can be extended for devices dominated by a Sch conduction. The capacitance of this zone, related to the dielectric constant of the interface,[16] was not considered here, as we are focusing our description on the low frequency regime. Other circuit representations of memristors can be found elsewhere.[19–22]

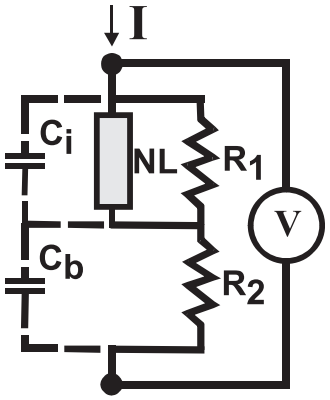

FIG. 4. Circuit elements proposed to represent the IV characteristics of bipolar memristors. A pure non-linear element (NL) and an ohmic resistor R_1 represent the interfacial elements while a second ohmic resistor R_2 in series represents the bulk. The interfacial (C_i) and bulk (C_b) capacitances have been included for completeness with dashed lines as their contribution is not relevant here because we are only considering the static response to electric fields.

The convenience of this circuit to describe the behavior of memristive interfaces was tested by reproducing the dynamical behavior of metal-YBCO interfaces[12] and by capturing the non-trivial IV characteristics of metal-manganite junctions.[13] In the case of devices with non-negligible bulk resistance, a second ohmic element in series (R_2) should be considered.

B. The case where the NL element is associated with a SCLC mechanism

We first analyze the simple case of an SCLC element without traps (Child's law)[23] in parallel with an ohmic resistor R_1. In this case, the current (I) dependence on applied voltage (V) corresponds to the following equation:

$$I = A\,V^2 + \frac{V}{R_1}, \tag{1}$$

with $A = \frac{9}{8}\frac{\mu\epsilon}{d^3}$, where μ is the carrier mobility, ϵ the static dielectric constant, and d the distance between contacts.

As shown in Fig. 5, γ increases asymptotically from 1 to 2 depending on the $A \times R_1$ factor. The saturation to 2 is obtained at lower voltages when increasing this factor.

Second, we consider the SCLC element only in series with the ohmic element R_2. In this case, the current I is related to the total voltage drop V by

$$I = A\,(V - IR_2)^2. \tag{2}$$

This second degree equation can be solved to extract the relationship between I and V in order to calculate the γ factor. As shown in Fig. 6, γ evolves from the pure SCLC value 2 at low voltages to the ohmic dependence 1 at higher voltages. The velocity of this evolution increases when increasing the $A \times R_2$ factor.

Finally, when both R_1 and R_2 are present, the relationship between I and V is obtained by solving Eq. (3). A superposition of both previous behaviors can be observed in Fig. 7. Here, the $A \times R_1$ controls the voltage where the γ

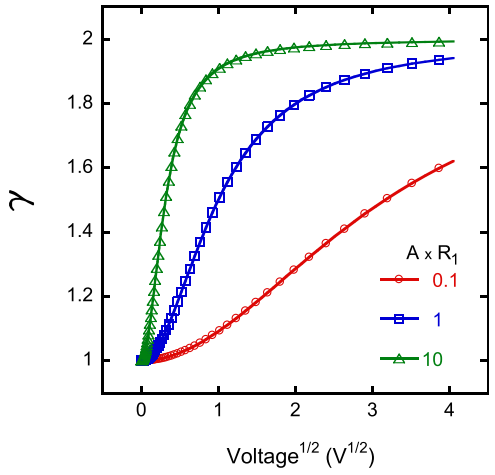

FIG. 5. γ representation for a SCLC conduction with an ohmic element R_1 in parallel. The $A \times R_1$ factor controls the voltage dependence of γ from an ohmic ($\gamma = 1$) to a SCLC ($\gamma = 2$) behavior.

peak is obtained (always with $\gamma \leq 2$), while $A \times R_1$ determines the rapidity to tend to an ohmic behavior when increasing the voltage.

$$I = A\,(V - IR_2)^2 + \frac{(V - IR_2)}{R_1}. \tag{3}$$

C. The case where the NL element is associated with a PF mechanism

When dealing with a NL element related to a PF mechanism in a circuit that includes both R_1 and R_2 (see Fig. 4), the relationship between the current I and the voltage V corresponds to the following implicit equation:

$$I = \left(\frac{V - IR_2}{R_1}\right)\left\{\frac{R_1}{R_{PF}}\exp\left[\frac{C(V - IR_2)^{1/2}}{k_B T}\right] + 1\right\}, \tag{4}$$

with

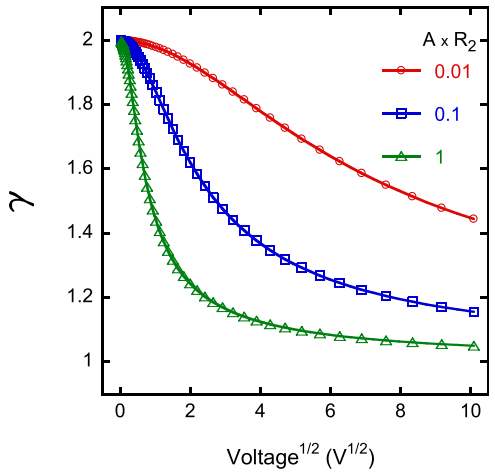

FIG. 6. γ representation for a SCLC conduction with an ohmic element R_2 in series. Here, the $A \times R_2$ factor regulates the voltage sensitivity of γ that evolves, with increasing the voltage, from a SCLC ($\gamma = 2$) to an ohmic ($\gamma = 1$) behavior.

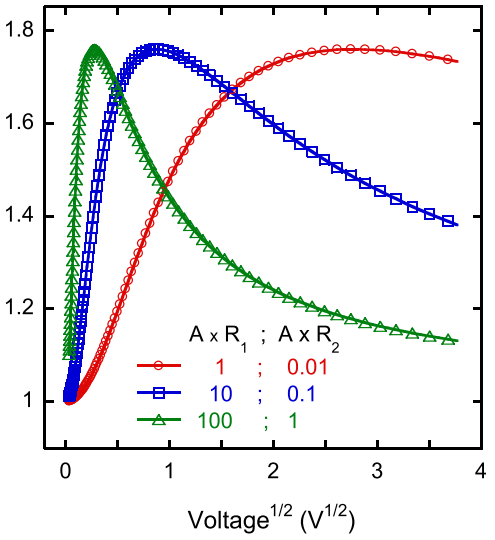

FIG. 7. γ representation for a SCLC conduction with an ohmic element R_1 in parallel and a second ohmic element R_2 in series. A peak can be observed, where the factor $A \times R_1$ determines its position and $A \times R_2$ its width.

$$R_{PF} = \frac{R_{ox}}{\exp\left(-\frac{\phi_B}{k_B T}\right)}, \quad C = \frac{q^{3/2}}{(\pi\epsilon' d)^{1/2}}, \quad R_{ox} = \frac{d}{Sqn_0\mu}, \tag{5}$$

where T is the temperature, k_B the Boltzmann constant, ϕ_B the trap energy level, q the electron's charge, S the conducting area, ϵ', n_0, and μ the real part of the dielectric constant, the density of carriers, and their mobility in the oxide, respectively, d the distance where the voltage drop is produced, and R_{PF} the resistance of the PF element when $V \mapsto 0$.

This equation should be solved numerically in order to determine the IV curves and to calculate the γ factor. As can be derived from Eq. (4), three different factors control the IV dependencies: $\frac{R_{PF}}{R_1}$, R_2, and $\frac{C}{T}$. The influence of each factor was analyzed (while maintaining constant the others) as shown in Figs. 8–10.

As can be observed in Fig. 8, the ohmic region at low voltages increases when increasing the ratio $\frac{R_{PF}}{R_1}$. This fact is associated with the weight in the conduction process of each element so that the ohmic region delays the PF contribution

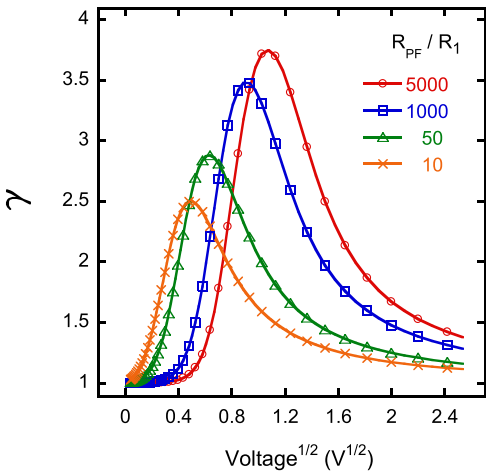

FIG. 8. γ representation for a PF element in parallel with an ohmic resistor (R_1) and in series with a second resistor (R_2). The γ curves are plotted for different R_{PF}/R_1 ratios.

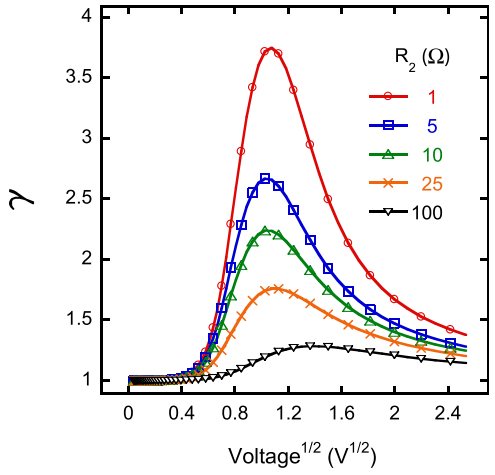

FIG. 9. γ representation for a PF element in parallel with an ohmic resistor (R_1) and in series with a second resistor (R_2). The γ curves are plotted for different R_2 values.

when $R_1 \ll R_{PF}$. With regard to the peak of γ, it is developed in the region of influence of the PF element and may reach values >2. In this way, if an increasing $\gamma > 2$ is observed when analyzing the γ plots of experimental data, the existence of an SCLC mechanism (Child's law) as the main NL element can be ruled out.

When $R_1 \leq R_{PF}$, R_1 becomes short-circuited by the PF element when increasing the voltage, and the overall behavior becomes asymptotically ohmic by the main contributions to the IV characteristics imposed by R_2.

When increasing R_2, the voltage region of the PF element influence is decreased in a way that the γ peak is reduced (eventually with values <2) and becomes wider, making it barely visible, as depicted in Fig. 9.

Finally, as shown in Fig. 10, when the ratio $\frac{C}{T}$ increases, the voltage width of the γ peak, which indicates the extension of the PF influence in the circuit behavior, is reduced. This figure points out the importance of performing IV measurements at different temperatures (see Ref. 14), as this can be a way to

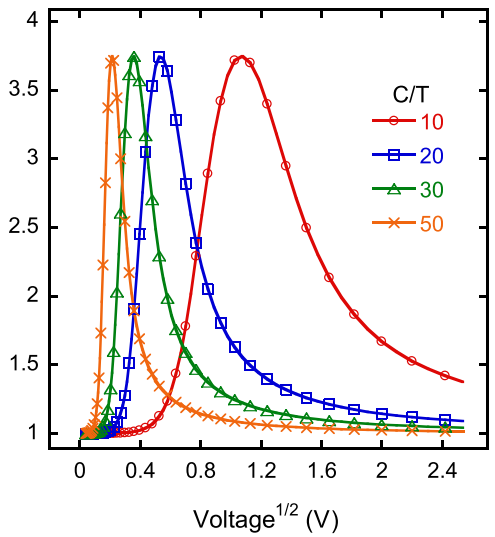

FIG. 10. γ representation for a PF element in parallel with an ohmic resistor (R_1) and in series with a second resistor (R_2). The γ curves are plotted for different C/T ratios.

determine (or to check) the temperature dependence of microscopic parameters, such as $\epsilon'(T)$ (from C) or ϕ_B (from the temperature dependence of R_{PF}), as well as of other parameters, such as R_1 or R_2, which can also be temperature dependent.

It is interesting to note that when performing the fits to the experimental data, the number of fitting parameters can be reduced if the low voltage resistance of the device is measured (usually called R_{rem}). For example, in the case of the PF element with the ohmic resistors R_1 and R_2, by analyzing Eq. (4) in the low voltage limit, it can be shown that $R_2 \simeq R_{rem} - (1/R_{PF} + 1/R_1)$.

These examples show the utility of the γ representation when dealing with the experimental curves measured at different temperatures: just by graphically analyzing the shape of this curve, the existence of a particular NL element can be determined as well as the necessity to include additional ohmic elements as R_1 and R_2. Then, the proper IV relation can be used in order to fit the data and to extract the microscopic parameters that govern the conduction mechanism of a device.

III. CONCLUSION

We have shown that the power exponent parameter γ plotted as a function of $V^{1/2}$ can be a useful tool to graphically determine the conduction mechanisms through an interface. This method becomes particularly interesting when the contribution to the conduction process comes from a combination of different elements, including a NL element in series and/or in parallel with ohmic ones. As this is the typical scenario found for some memristive interfaces, the idea is to ease the determination of these elements in order to obtain relevant microscopic information by fitting their IV characteristics with the corresponding expression.

ACKNOWLEDGMENTS

We would like to thank the financial support by CONICET Grant Nos. PIP 112-200801-00930, PICT 2013-0788, and UBACyT 20020130100036BA (2014-2017). We are grateful to A. Schulman, M. Boudard, K. Daoudi, and T. Tsuchiya and to I. Abinzano, C. Peralta, A. Kleiman, and A. Márquez for providing the experimental data shown in Figs. 2 and 3, respectively. We also acknowledge Dr. V. Bekeris for a critical reading of the manuscript.

[1]S. M. Sze and K. K. Ng, *Physics of Semiconductor Devices* (John Wiley & Sons, 2007), Chap. 3–4.
[2]F.-Ch. Chiu, Adv. Mater. Sci. Eng. **2014**, 578168.
[3]R. Waser and M. Aono, Nat. Mater. **6**, 833 (2007).
[4]D. B. Strukov, G. S. Snider, D. R. Stewart, and R. S. Williams, Nature **453**, 80 (2008).
[5]A. Sawa, Mater. Today **11**, 28 (2008).
[6]G. W. Dietz, W. Antöhler, M. Klee, and R. Waser, J. Appl. Phys. **78**, 6113–6121 (1995).
[7]D. S. Shang, J. R. Sun, L. Shi, J. Wang, Z. H. Wang, and B. G. Shen, Appl. Phys. Lett. **94**, 052105 (2009).
[8]A. Schulman, L. F. Lanosa, and C. Acha, J. Appl. Phys. **118**, 044511 (2015).
[9]M. Nardone, M. Simon, I. V. Karpov, and V. G. Karpov, J. Appl. Phys. **112**, 071101 (2012).
[10]A. Bozhko, M. Shupegin, and T. Takagi, Diamond Relat. Mater. **11**, 1753 (2002).
[11]V. Mikhelashvili, G. Eisenstein, V. Garber, S. Fainleib, G. Bahir, D. Ritter, M. Orenstein, and A. Peer, J. Appl. Phys. **85**, 6873 (1999).
[12]C. Acha, J. Phys. D: Appl. Phys. **44**, 345301 (2011).

[13]F. Gomez-Marlasca, N. Ghenzi, A. G. Leyva, C. Albornoz, D. Rubi, P. Stoliar, and P. Levy, J. Appl. Phys. **113**(14), 144510 (2013).
[14]C. Acha, A. Schulman, M. Boudard, K. Daoudi, and T. Tsuchiya, Appl. Phys. Lett. **109**, 011603 (2016).
[15]W. Román Acevedo, C. Acha, M. J. Sánchez, P. Levy, and D. Rubi, Appl. Phys. Lett. **110**, 053501 (2017).
[16]P. Lunkenheimer, V. Bobnar, A. V. Pronin, A. I. Ritus, A. A. Volkov, and A. Loidl, Phys. Rev. B **66**, 052105 (2002).
[17]I. Abinzano, C. Peralta, A. Kleiman, A. Márquez, D. R. Vega, and C. Acha, "Resistive switching in Pt/TiO_2/Ti devices grown by cathodic arc" (to be published).
[18]D.-H. Kwon, K. M. Kim, J. H. Jang, J. M. Jeon, M. H. Lee, G. H. Kim, X.-S. Li, G.-S. Park, B. Lee, S. Han, M. Kim, and C. S. Hwang, Nat. Nanotechnol. **5**, 148 (2010).
[19]J. Blasco, N. Ghenzi, J. Suae, P. Levy, and E. Miranda, IEEE Electron Device Lett. **35**, 390–392 (2014).
[20]J. Blasco, N. Ghenzi, J. Suñé, P. Levy, and E. Miranda, Microelectron. Reliab. **55**, 1–14 (2015).
[21]A. G. Radwan and M. E. Fouda, *On the Mathematical Modeling of Memristor, Memcapacitor, and Meminductor* (Springer, 2016).
[22]I. Vourkas and G. Sirakoulis, *Memristor-Based Nanoelectronic Computing Circuits and Architectures* (Springer, 2016).
[23]P. Mark and W. Helfrich, J. Appl. Phys. **33**, 205 (1962).